Comparing Adjoint and Ensemble Sensitivity Analysis with Applications to Observation Targeting

Brian Ancell[1] & Gregory J. Hakim

University of Washington, Seattle, WA

Submitted to *Monthly Weather Review*

March 15, 2007

[1] *Corresponding Author:*
Brian Ancell
Department of Atmospheric Sciences, Box 351640
University of Washington
Seattle, WA 98195-1640
E-mail: bancell@atmos.washington.edu

Abstract

The sensitivity of numerical weather forecasts to small changes in initial conditions is estimated using ensemble samples of analysis and forecast errors. Ensemble sensitivity is defined here by linear regression of analysis errors onto a given forecast metric. We show that ensemble sensitivity is proportional to the projection of the analysis-error covariance onto the adjoint sensitivity field. Furthermore, the ensemble sensitivity approach proposed here involves a small calculation that is easy to implement.

Ensemble and adjoint-based sensitivity fields are compared for a representative wintertime flow pattern near the West Coast of North America for a 90-member ensemble of independent initial conditions derived from an ensemble Kalman filter. The forecast metric is taken for simplicity to be the 24-hr forecast of sea-level pressure at a single point in western Washington state. Results show that adjoint and ensemble sensitivities are very different in terms of location, scale, and magnitude. Adjoint sensitivity fields reveal mesoscale lower-tropospheric structures that tilt strongly upshear, whereas ensemble sensitivity fields emphasize synoptic-scale features that tilt modestly throughout the troposphere and are associated with significant weather features at the initial time.

Optimal locations for targeting can easily be determined from ensemble sensitivity, and results indicate that the primary targeting locations are located away from regions of greatest adjoint and ensemble sensitivity. We show that this method of targeting is similar to previous ensemble-based methods that estimate forecast-error variance reduction, but easily allows for the application of statistical confidence measures to deal with sampling error.

1. Introduction

Sensitivity analysis is a central problem in predictability research that involves determining how changes to an initial condition affect a later forecast. In general this problem involves nonlinear systems, although it is common practice to linearize about a reference state-space forecast trajectory. One linear approach to sensitivity analysis involves solving for changes in the forecast that result from independently perturbing every degree of freedom in the initial conditions. This allows one to determine the change in a forecast to arbitrary changes in the initial conditions through a linear combination of the independent perturbations. Such an approach is impractical for systems with a large number of degrees of freedom, such as in numerical weather prediction. Another linear approach is adjoint sensitivity, where a single integration of the adjoint model achieves the same goal, limited to a scalar metric of the forecast field. Here we explore an ensemble approach to estimating forecast sensitivity, compare it to adjoint sensitivity, and explore its potential for targeting observations.

Ensemble sensitivity was first explored by Hakim and Torn (2006), who examined the linear relationship between a 24-hr ensemble forecast of the central pressure of an extratropical cyclone and the initial-condition state variables. They found that the linear relationships were synoptic-scale, deep, and sensibly related (mainly phase differences) to the primary synoptic structures. These patterns contrast with typical adjoint sensitivity patterns and singular vectors for extratropical cyclones, which have been found predominantly in the lower troposphere, with large vertical tilts (Errico and Vukicevic 1992, Langland et al. 1995, Rabier et al. 1996, Zou et al. 1998, Hoskins et al. 2000). Here we extend the ensemble approach and explore it's relationship to adjoint sensitivity and to other ensemble-based sensitivity methods.

Sensitivity analysis can be used to improve forecasts through targeting observations. These observations are meant to supplement the existing observing network in locations where the forecast is particularly sensitive to new information. Strategies for identifying

locations for targeting should incorporate analysis error, observation error, dynamical error growth, and the data assimilation method used to assimilate the targeted observations (Berliner et al. 1999). Two approaches to the targeting problem have been proposed and tested in field programs: adjoint-sensitivity or singular vector methods (Buizza and Montani 1999, Gelaro et al. 1999, Langland et al. 1999), and ensemble-based methods (Bishop et al. 2001, Hamill and Snyder 2002). Here we explore an ensemble-based approach that, in the appropriate norm, is similar to previous ensemble-based methods, but also relates directly to adjoint sensitivity and is easily understood and calculated in terms of linear regression.

The outline of the paper is as follows. Section 2 reviews adjoint and ensemble sensitivity theory, including relationships to the ensemble transform Kalman filter (ETKF). This theory is applied to a case study, with the details of the method given in section 3 and the results in section 4. Section 5 reviews targeting applications, and section 6 provides a concluding summary.

2. Adjoint and Ensemble Sensitivity Background

2.a Adjoint Sensitivity Formulation

A detailed description of the adjoint methodology can be found in LeDimet and Talagrand (1986) and a brief review is provided here. The temporal evolution of a discrete dynamical system, represented by state vector $\mathbf{x}$, is described by

$$\frac{d\mathbf{x}}{dt} = \mathbf{F}(\mathbf{x}), \tag{1}$$

where $\mathbf{F}(\mathbf{x})$ is, in general, a vector-valued, nonlinear function. Linearizing $\mathbf{F}(\mathbf{x})$ about a reference trajectory, the evolution of an initial disturbance can be expressed as a map of the form

$$\delta\mathbf{x}_t = \mathbf{R}_{t,t_0}\delta\mathbf{x}_0, \tag{2}$$

where the initial and final times are denoted by t_0 and t, respectively, and $\mathbf{R}_{t,t_0}$ is the

resolvant matrix, which maps the perturbation column vector at initial time, $\delta\mathbf{x}_0$, into the perturbation column vector at forecast time, $\delta\mathbf{x}_t$. These perturbation vectors are deviations from the nonlinear basic-state trajectory, which must first be determined before evaluating the linear perturbation evolution. Typically the action of the resolvant is estimated by the integration of a tangent linear model (TLM) over a set of discrete time steps; e.g. $\mathbf{R}_{t,t_0} = \mathbf{R}_{t,t-\delta t} \cdots \mathbf{R}_{t_i+\delta t,t_i} \cdots \mathbf{R}_{t_0+\delta t,t_0}$.

We introduce a scalar metric, J, referred to as the response function, which is some arbitrary function of the forecast state at time t. This response function is chosen to measure a feature and/or location of interest. For small changes to the forecast at time t, J may be estimated by a truncated Taylor expansion about the control solution

$$J(\mathbf{x}_t + \delta\mathbf{x}_t) = J(\mathbf{x}_t) + \left[\frac{\partial J}{\partial \mathbf{x}_t}\right]^{\mathrm{T}} \delta\mathbf{x}_t + \cdots, \tag{3}$$

and the change in J is therefore approximated by

$$\delta J = J(\mathbf{x}_t + \delta\mathbf{x}_t) - J(\mathbf{x}_t) \doteq \left[\frac{\partial J}{\partial \mathbf{x}_t}\right]^{\mathrm{T}} \delta\mathbf{x}_t. \tag{4}$$

Using (2), this expression becomes

$$\delta J \doteq \left[\frac{\partial J}{\partial \mathbf{x}_t}\right]^{\mathrm{T}} \mathbf{R}(t,t_0)\delta\mathbf{x}(t_0), \tag{5}$$

and, with the algebraic properties of the transpose, this may be written as

$$\delta J \doteq \left[\mathbf{R}_{t,t_0}^{\mathrm{T}} \frac{\partial J}{\partial \mathbf{x}_t}\right]^{\mathrm{T}} \delta\mathbf{x}(t_0). \tag{6}$$

Recall that the resolvant is composed of a product of steps, so that the transpose operation flips in time the order of this sequence for the adjoint model

$$\mathbf{R}_{t,t_0}^{\mathrm{T}} = \mathbf{R}_{t_0+\delta t,t_0}^{\mathrm{T}} \cdots \mathbf{R}_{t_i+\delta t,t_i}^{\mathrm{T}} \cdots \mathbf{R}_{t,t-\delta t}^{\mathrm{T}}. \tag{7}$$

Thus the adjoint works backward in time, mapping the "sensitivity gradient" backward in time to t_0, yielding the sensitivity gradient with respect to $\mathbf{x}(t_0)$, $\frac{\partial J}{\partial \mathbf{x}_0}$:

$$\mathbf{R}_{t,t_0}^{\mathrm{T}} \frac{\partial J}{\partial \mathbf{x}_t} = \frac{\partial J}{\partial \mathbf{x}_0}. \tag{8}$$

From (6), we see that (8) links the change in the metric at the solution time to the adjoint sensitivity at the initial time; that is, how changes to the initial condition affect the forecast, as measured by J

$$\delta J = \left[\frac{\partial J}{\partial \mathbf{x}_0}\right]^{\mathrm{T}} \delta \mathbf{x}_0. \tag{9}$$

The adjoint sensitivity with respect to the initial state will hereafter be referred to as $\frac{\partial J}{\partial \mathbf{x}_0}$.

2.b Ensemble Sensitivity and its Relationship to Adjoint Sensitivity

Ensemble-based sensitivity analysis employs independent samples of the state at the initial and final time to estimate statistically how changes to the initial condition affect the forecast metric. Although ensemble sampling is used in practice, we note that the theoretical arguments given subsequently are more general, and do not in fact depend on ensemble sampling; nevertheless, we shall refer to the approach generically as "ensemble sensitivity." The relationship between ensemble and adjoint sensitivity analysis is derived by starting with (9), right-multiplying by $\delta \mathbf{x}_0^{\mathrm{T}}$, and taking the expected value (curly brackets)

$$\left\{ \delta J \delta \mathbf{x}_o^{\mathrm{T}} = \left[\frac{\partial J}{\partial \mathbf{x}_0}\right]^{\mathrm{T}} \delta \mathbf{x}_0 \delta \mathbf{x}_0^{\mathrm{T}} \right\}. \tag{10}$$

Since $\left[\frac{\partial J}{\partial \mathbf{x}_0}\right]^{\mathrm{T}}$ is a deterministic quantity applying to the control trajectory, we may rewrite this equation as

$$\left\{ \delta J \delta \mathbf{x}_o^{\mathrm{T}} \right\} = \left[\frac{\partial J}{\partial \mathbf{x}_0}\right]^{\mathrm{T}} \mathbf{A}, \tag{11}$$

where $\left\{ \delta J \delta \mathbf{x}_o^{\mathrm{T}} \right\}$ is the covariance of the forecast metric with the initial conditions and $\mathbf{A} = \left\{ \delta \mathbf{x}_0 \delta \mathbf{x}_0^{\mathrm{T}} \right\}$ is the initial-time error covariance matrix. Note that we have assumed that the initial-time perturbations, $\delta \mathbf{x}_0$, have zero mean. Taking the transpose of (11), and noting that $\mathbf{A}$ is symmetric, reveals that the forecast-metric–initial-condition covariance represents the projection of the analysis-error covariance field onto the adjoint sensitivity field.

The covariance alone does not give the linear-regression relationship between the response function and the initial state, and we consider two approaches. One approach,

simultaneous multivariate regression, is obtained by right multiplying (11) by $\mathbf{A}^{-1}$, which recovers the adjoint sensitivity within sampling error:

$$\left\{\delta J \delta \mathbf{x}_o^{\mathrm{T}}\right\} \mathbf{A}^{-1} = \left[\frac{\partial J}{\partial \mathbf{x}_0}\right]^{\mathrm{T}}. \tag{12}$$

In practice, $\mathbf{A}^{-1}$ is a large matrix that is difficult to invert and, if derived from a small ensemble sample, is not unique. This motivates a second approach, which is univariate regression. In this case, the response function is regressed onto all initial degrees of freedom independently by

$$\left[\frac{\partial J_e}{\partial \mathbf{x}_0}\right]^{\mathrm{T}} \equiv \{J, \delta \mathbf{x}_o\} \mathbf{D}^{-1}. \tag{13}$$

Here $\mathbf{D}$ is a diagonal matrix with initial-time error variance (i.e. diagonal entries of $\mathbf{A}$, and zeros elsewhere), and $\left[\frac{\partial J_e}{\partial \mathbf{x}_0}\right]$ is the ensemble sensitivity. Using (11), it can be shown that the relationship to adjoint sensitivity in this case is

$$\frac{\partial J_e}{\partial \mathbf{x}_0} = \mathbf{D}^{-1} \mathbf{A} \frac{\partial J}{\partial \mathbf{x}_0}. \tag{14}$$

This approach, which we will hereafter refer to as ensemble sensitivity, has the advantage that the inverse of the matrix $\mathbf{D}$ is trivial to calculate, and it offers the opportunity to address sampling issues in the calculation of $\mathbf{A}$, such as through statistical confidence estimates or "localization" (e.g. Whitaker and Hamill 2002). We note that in the limit of diagonal $\mathbf{A}$, ensemble and adjoint sensitivities are equivalent.

In practice, the expectation integrals are approximated using ensemble samples of size M. Denoting the ensemble state matrix by $\delta \mathbf{X}$, where ensemble member states are column vectors with the ensemble-mean removed, the ensemble-estimated covariance is given by

$$\mathbf{A} = \frac{1}{M-1} \delta \mathbf{X} \delta \mathbf{X}^{\mathrm{T}}. \tag{15}$$

Typically, $M \ll N$ so that $\mathbf{A}$ is rank-deficient and $\mathbf{A}^{-1}$ is not unique. Appendix A illustrates how $\mathbf{A}^{-1}$ can be approximated through singular vector decomposition in order to calculate the adjoint sensitivities from (12). Although non-unique and computationally intensive, this methodology could provide case-dependent adjoint sensitivity fields utilizing complex physics for which the tangent linear and adjoint models do not explicitly exist.

2.c Ensemble Sensitivity Method for Targeting Observations

Here we demonstrate the usefulness of ensemble sensitivities for the targeting observation problem. We assume that a Kalman filter is used for assimilating new observations, which is optimal under linear dynamics and unbiased Gaussian error statistics. For an ensemble of size M, the ensemble estimate of the response function can be represented as a row vector, $\mathbf{J}$. Similarly, removing the ensemble mean from $\mathbf{J}$ gives the row vector of ensemble perturbations, $\delta\mathbf{J}$, the variance of which is defined by

$$\sigma = \frac{1}{M-1}\delta\mathbf{J}\delta\mathbf{J}^{\mathrm{T}}. \tag{16}$$

Substituting the expression for $\delta\mathbf{J}$ from equation (9), with $\delta\mathbf{x}_0$ replaced by $\delta\mathbf{X}_0$, into equation (16), and using the definition for the ensemble estimate of $\mathbf{A}$, the variance of the response function becomes

$$\sigma = \left[\frac{\partial J}{\partial \mathbf{x}_0}\right]^{\mathrm{T}} \mathbf{A} \left[\frac{\partial J}{\partial \mathbf{x}_0}\right]. \tag{17}$$

When observations are assimilated, the prior error covariance matrix, $\mathbf{B}$, is updated by

$$\mathbf{A} = (\mathbf{I} - \mathbf{K}\mathbf{H})\mathbf{B}. \tag{18}$$

The Kalman gain matrix is given by

$$\mathbf{K} = \mathbf{B}\mathbf{H}^{\mathrm{T}}\left[\mathbf{H}\mathbf{B}\mathbf{H}^{\mathrm{T}} + \mathbf{R}\right]^{-1}, \tag{19}$$

where $\mathbf{H}$ is a linearized observation operator that maps the background to the observations, $\mathbf{I}$ is the identity matrix, and $\mathbf{R}$ is the observation error covariance matrix. For sufficiently small analysis increments, the adjoint sensitivity field derived for the ensemble-mean forecast remains valid as the leading-order approximation to the sensitivity of the response function to changes in the initial conditions.

Consider now the targeting situation where new observations are to be taken. Let $\mathbf{A}$ represent the analysis-error covariance matrix after the assimilation of the routine observations, and $\mathbf{A}'$ represent the analysis-error covariance matrix after the assimilation of

the new, hypothetical, targeted observations. The reduction in response function variance resulting from the assimilation of the new observations is

$$\delta\sigma = \left[\frac{\partial J}{\partial \mathbf{x}_0}\right]^{\mathrm{T}} (\mathbf{A} - \mathbf{A}') \left[\frac{\partial J}{\partial \mathbf{x}_0}\right]. \tag{20}$$

Using (18) and (19), and noting that $\mathbf{A}$ is now the prior error covariance matrix gives

$$\delta\sigma = \left[\frac{\partial J}{\partial \mathbf{x}_0}\right]^{\mathrm{T}} \mathbf{A}\mathbf{H}^{\mathrm{T}}\mathbf{E}^{-1}\mathbf{H}\mathbf{A} \left[\frac{\partial J}{\partial \mathbf{x}_0}\right], \tag{21}$$

where $\mathbf{E}$ is the innovation error covariance matrix, $(\mathbf{H}\mathbf{A}\mathbf{H}^{\mathrm{T}} + \mathbf{R})$. Using (14), and the properties of the transpose, gives

$$\delta\sigma = \left(\mathbf{H}\mathbf{D}\frac{\partial J_e}{\partial \mathbf{x}_0}\right)^{\mathrm{T}} \mathbf{E}^{-1} \left(\mathbf{H}\mathbf{D}\frac{\partial J_e}{\partial \mathbf{x}_0}\right). \tag{22}$$

Note that $\delta\sigma$ is positive definite: observations always act to reduce forecast-metric variance. All that is needed to evaluate (22) is the error covariance matrix of the targeted observations and the variance-weighted ensemble sensitivities, both of which are known without taking the actual measurements. Variance-weighted ensemble sensitivity is simply the covariance between the forecast metric and the model initial-time state variables, making the calculation of (22) straightforward. In the limit of a single observation, $\mathbf{E}$ becomes scalar and (22) reduces to the square of the covariance between the forecast metric and the model initial conditions, interpolated to the observation location by $\mathbf{H}$ and normalized by the innovation variance. In order to determine the targeting location for a new observation, we will consider the special case where the new observations are evaluated at the n model grid points. In this case, the reduction in variance of the response function due to a hypothetical observation considered independently with respect to each model state variable can be calculated without $\mathbf{H}$. This calculation involves n evaluations of $\delta\sigma$, which is computationally inexpensive. The grid point with the largest value of $\delta\sigma$ is the location assigned the highest targeting priority. We emphasize that the actual value of the observation is inconsequential in this formulation, only the error variance of the observation must be known.

Once the first targeted observation location has been determined, additional targeting locations may be found by serial assimilation. Using the methodology outlined above, it is straightforward to determine the change in the response function variance given that the observation with the largest value from equation (22) was assimilated. In general, the variance reduction conditioned on the assimilation of $i-1$ previous hypothetical observations is given by

$$\delta\sigma_i = \left[\frac{\partial J}{\partial \mathbf{x}_0}\right]^{\mathrm{T}} \mathbf{K}_i \mathbf{H}_i \mathbf{A}_{i-1} \left[\frac{\partial J}{\partial \mathbf{x}_0}\right]. \tag{23}$$

Note that $\mathbf{K}_i = \mathbf{A}_{i-1}\mathbf{H}_i^{\mathrm{T}}\left[\mathbf{H}_i\mathbf{A}_{i-1}\mathbf{H}_i^{\mathrm{T}} + \mathbf{R}_i\right]^{-1}$ is a function of the observation operator and observation error covariance for the ith set of observations, which are known *a priori*, and the analysis error covariance matrix, $\mathbf{A}_{i-1}$ for all previous sets of observations.

By recursively substituting for $\mathbf{K}_i$ and $\mathbf{A}_{i-1}$, one can show that (23) may always be reduced to a function of the original analysis error covariance, $\mathbf{A}_0$. For example, the potential impact of a second set of observations, given the reduction in the error variance from a first set, may be estimated by

$$\delta\sigma_2 = \left[\mathbf{D}_0\frac{\partial J_e}{\partial \mathbf{x}_0}\right]^{\mathrm{T}} \left[\mathbf{H}_2^{\mathrm{T}} - \mathbf{H}_1^{\mathrm{T}}\mathbf{E}_1^{-1}\mathbf{H}_1\mathbf{A}_0\mathbf{H}_2^{\mathrm{T}}\right]\mathbf{E}_2^{-1}\left[\mathbf{H}_2 - \mathbf{H}_2\mathbf{A}_0\mathbf{H}_1^{\mathrm{T}}\mathbf{E}_1^{-1}\mathbf{H}_1\right]\left[\mathbf{D}_0\frac{\partial J_e}{\partial \mathbf{x}_0}\right], \tag{24}$$

where $\mathbf{E}_1 = \mathbf{H}_1\mathbf{A}_0\mathbf{H}_1^{\mathrm{T}} + \mathbf{R}_1$ is the innovation covariance matrix based on the first set of hypothetical observations and $\mathbf{E}_2 = \mathbf{H}_2\mathbf{A}_1\mathbf{H}_2^{\mathrm{T}} + \mathbf{R}_2$ is the innovation covariance matrix based on the second set. We note that $\mathbf{E}_2$ can be expressed in terms of $\mathbf{A}_0$ alone,

$$\mathbf{E}_2 = \mathbf{H}_2\mathbf{A}_0\mathbf{H}_2^{\mathrm{T}} - \mathbf{H}_2\mathbf{A}_0\mathbf{H}_1^{\mathrm{T}}\mathbf{E}_1^{-1}\mathbf{H}_1\mathbf{A}_0\mathbf{H}_2^{\mathrm{T}} + \mathbf{R}_2. \tag{25}$$

For a single observation, $\mathbf{E}_i$ is scalar and therefore the inverse is trivial to evaluate. Thus, it is computationally inexpensive to calculate a relatively small number of hypothetical observations that reduce the variance the most given the simultaneous assimilation of their predecessors.

Determining regions for real-time targeting requires sufficient time to deploy adaptive observing platforms. Thus, the ensemble sensitivities used to determine targeting locations must be formulated by regressing the forecast response function against a short-range

forecast, such as 6 hours. Since routine observations may also exist at this forecast time, their affect on the analysis and forecast metric should be determined prior to calculating the ensemble sensitivity. This may be accomplished by using an ensemble Kalman filter to update the ensemble perturbations for the short-term forecast, and for the forecast response function, prior to determining the ensemble sensitivity. However, this method is computationally intensive and may pose timing problems for real-time applications. A much simpler way to consider future routine observations is to treat them in the same manner that a first set of observations was considered serially with equation (24). This method would easily be applicable in real-time for a relatively small number of observations, but may become too computationally intensive for a large number of observations. Since many observations are likely redundant, the large number of observations may be thinned in order to produce targeting locations in real time, although this may degrade the accuracy of the variance reduction values, and such a thinning method has not yet been developed. These limitations reveal the disadvantages of the ensemble sensitivity method for real-time observation targeting applications.

In addition to targeting, when an observation value is known, its impact on the value of the ensemble-mean forecast metric can be estimated by methods similar to those for variance reduction discussed above. This is useful, for example, when the value of targeted observations become available, or when selectively sampling from a large set of observations in order to thin the set to those having the largest impact on the forecast metric. Langland and Baker (2004) developed observation sensitivity fields with the adjoints of both a numerical model and a variational data assimilation system with a static background error covariance matrix in order to assess observational impact of various assimilated observations. Langland and Baker (2004) show that the transpose of the innovation vector multiplied by the observation sensitivity vector yields a sum over the contribution from each observation to the total change in the forecast metric. Thus, the impact of each observation on the metric for the simultaneous assimilation of a large number of observations can be assessed.

For the Kalman filter, the analysis increment for the new observations is given by

$$\delta \mathbf{x}_0 = \mathbf{K} \left[\mathbf{y} - \mathcal{H}(\mathbf{x}_0) \right]. \tag{26}$$

From (9), the change in the response function for the ensemble mean is

$$\delta J = \left[\frac{\partial J}{\partial \mathbf{x}_0} \right]^{\mathrm{T}} \mathbf{K} \left[\mathbf{y} - \mathcal{H}(\mathbf{x}_0) \right]. \tag{27}$$

Using (14), (27) may be re-written as

$$\delta J = \left[\mathbf{HD} \frac{\partial J_e}{\partial \mathbf{x}_0} \right] \left[\mathbf{HAH}^{\mathrm{T}} + \mathbf{R} \right]^{-1} \left[\mathbf{y} - \mathcal{H}(\mathbf{x}_0) \right]. \tag{28}$$

Equation (28) recovers the same result found in Langland and Baker (2004), except that ensemble sensitivities are used here instead of the AECM and adjoint sensitivity. Such use of ensemble sensitivities requires no adjoint model as in Langland and Baker (2004), because the adjoint sensitivity field is implicit in the ensemble sensitivity values. Evaluating (28) amounts to interpolating the variance-weighted ensemble sensitivity values to observation space, or equivalently, calculating the covariances between the metric and the observation estimates, and then multiplying the results by the normalized observation innovation. As in Langland and Baker (2004), a scalar term is the result, which is composed of a set of terms that are associated with each observation assimilated. If there are relatively few observations compared to the number of degrees of freedom for the model, then (28) allows for a computationally efficient assessment of observational impact.

2.d Relationship to the ETKF method

Bishop et al. (2001) and Hamill and Snyder (2002) both develop expressions for the change in the forecast error covariance matrix due to targeted observations, which Bishop et al. (2001) refer to as the ETKF signal covariance matrix. This reduction in the forecast error covariance matrix (FECM) is (in our notation)

$$\mathbf{S} = \mathbf{R}_{t,t_0} \mathbf{AH}^{\mathrm{T}} \left[\mathbf{HAH}^{\mathrm{T}} + \mathbf{R} \right]^{-1} \mathbf{HAR}_{t,t_o}^{\mathrm{T}}. \tag{29}$$

Expanding (21) we get

$$\delta\sigma = \left[\frac{\partial J}{\partial \mathbf{x}_t}\right]^{\mathrm{T}} \mathbf{R}_{t,t_0}\mathbf{A}\mathbf{H}^{\mathrm{T}}\left[\mathbf{H}\mathbf{A}\mathbf{H}^{\mathrm{T}} + \mathbf{R}\right]^{-1}\mathbf{H}\mathbf{A}\mathbf{R}^{\mathrm{T}}_{t,t_o}\left[\frac{\partial J}{\partial \mathbf{x}_t}\right], \tag{30}$$

so that the relationship to the reduction in FECM to the ETKF method is

$$\delta\sigma = \left[\frac{\partial J}{\partial \mathbf{x}_t}\right]\mathbf{S}\left[\frac{\partial J}{\partial \mathbf{x}_t}\right]^{\mathrm{T}}. \tag{31}$$

By choosing a forecast metric *a priori*, the ensemble sensitivity method essentially localizes the variance reduction to the chosen metric. The equivalence of the variance reduction in a single degree of freedom can be realized from (31) by taking the forecast-time adjoint sensitivity to be one for a single degree of freedom and zero elsewhere. In this case, a single diagonal element of $\mathbf{S}$ is the result, revealing the reduction in variance of the one degree of freedom. In general, any metric defined by a linear transformation and/or linear combination of state variables will yield a result that is statistically equivalent to the ETKF.[1] One case where ensemble sensitivity yields results distinct from the ETKF is for nonlinear forecast metrics; however, we note that the link to adjoint sensitivity is also lost in this case.

Conceptually, the ensemble sensitivity method involves simple linear regression, whereas the ETKF requires the determination of a transform matrix. Furthermore, as we have shown, ensemble sensitivity links naturally to adjoint sensitivity. Finally, we note that the ensemble method described here also allows straightforward inclusion of statistical confidence measures to address sampling error; application of such a test will be demonstrated subsequently.

[1] This is true of all small-ensemble approximations: different ensemble samples yield the same covariance matrix due to the large null space.

3. Methodology

3.a Experimental Setup

A 90-member ensemble sample of analyses is taken from a limited-area ensemble Kalman filter (EnKF) system that runs operationally at the University of Washington. This system employs the Weather Research and Forecasting (WRF) model on a 6-hour update cycle using observations from satellite-derived winds, aircraft, radiosonde, buoy, ship, and land-based surface stations.

Ideally the model used for cycling the data assimilation system would also be used for the sensitivity analysis, but lacking an adjoint version of the WRF model, we instead adopted the PSU-NCAR MM5 model. Ensemble initial conditions were linearly interpolated from the WRF grid to the MM5 grid. Once interpolated to the MM5 grid, all 90 members are advanced 24 hours with the MM5 nonlinear forward model. Although the EnKF system from which the initial conditions are derived uses independent boundary conditions for each ensemble member (Torn et al. 2006), here the lateral boundary conditions are fixed for all members to the Global Forecast System (GFS) forecasts.

The response function J, defined as the lowest sigma level perturbation pressure at a single point, is linearly regressed onto the initial conditions to give the ensemble sensitivity field. Results for ensemble sensitivity derived from the MM5 ensemble and the original WRF ensemble yielded similar results throughout the model domain (not shown), suggesting that for this case, the use of deterministic boundary conditions instead of time-varying boundary conditions has little impact on the ensemble sensitivity values.

In order to calculate adjoint sensitivity, the ensemble-mean initial condition is first integrated with the nonlinear forward model; this trajectory serves as the basic state for the adjoint sensitivity calculation. The adjoint model is then integrated backward in time from the gradient of the response function with respect to the model variables at the forecast time. The adjoint model is based on version 3 of the MM5 model, as described in Ruggiero et al. (2002).

All model physics are consistent throughout this set of experiments. The nonlinear forecasts for the ensemble members, the nonlinear basic state trajectory for the adjoint run, and the adjoint model all used Anthes-Kuo cumulus parameterization, the Burk-Thompson planetary boundary layer scheme, the simple-precipitation explicit-moisture scheme, and the simple cooling radiation scheme. All experiments are performed on the same model domain at 45-km grid spacing with 33 vertical levels.

3.b. Synoptic Overview

Experiments pertain to the flow situation that occurred during the 24-hr period from 1200 UTC 3 February to 1200 UTC 4 February 2005. Fig. 1 shows the 00, 12, and 24-hr ensemble-mean forecasts of 500-hPa geopotential heights and absolute vorticity, and Fig. 2 shows the 925-hPa temperature and sea-level pressure (SLP) forecasts at the same times. For future reference, we note that the grid point defining the response function J (24-hr SLP forecast) is given by the black dot in Fig. 2.

At 1200 UTC 3 February, a large trough along 150° W dominated the 500-hPa field, while at the surface an occluded cyclone is found in the Gulf of Alaska and high pressure off the coast of the Pacific Northwest. Two low-level baroclinic zones existed at this time, one extending southwest from Washington, and another rotating around the occluded cyclone, extending southwest from southeastern Alaska.

At 0000 UTC 4 February, it appears that the 500 hPa trough began to interact with the northernmost low-level baroclinic zone, causing a cyclone to subsequently develop near 60° N, 140° W. At 1200 UTC 4 February, the cyclone was positioned over the Queen Charlotte Islands off the central British Columbia coast, and the trough aloft was just west of the North American coastline. Although the most vigorous portion of the 500 hPa trough was just west of the location of the response function location, no significant surface features are apparent at this location.

4 Results

4.a. Structure of Adjoint Sensitivities

The adjoint sensitivity of the response function J with respect to temperature at the initial time for sigma levels 7 (300 hPa), 12 (500 hPa), and 22 (850 hPa) is given in Fig. 3. Sensitivity decreases below 850 hPa to near zero near the surface. Regions of sensitivity are localized, small-scale structures that tilt strongly upshear in the vertical. Specifically, the dominant pattern is a wave-like structure that first appears at 500 hPa near 37° N, 150° W and tilts northeastward with decreasing height along the synoptic-scale flow aloft to become the sole significant feature at 850 hPa. These regions of significant lower-tropospheric adjoint sensitivities are not closely located to the significant pressure disturbances at the initial time, but rather the southern baroclinic zone. The maximum value in the sensitivity field of about 0.8 Pa/K indicates that a unit temperature perturbation at that point changes the value of the response function by 0.8 Pa. The adjoint sensitivity of J with respect to geopotential height exhibits similar structure to temperature, but with opposite sign (Fig. 5). The sensitivity of J with respect to geopotential height is a derived variable, and was obtained at each model grid point by multiplying the sensitivity with respect to pressure by the hydrostatic relation. The maximum value of about 0.006 Pa/m, implies that raising the geopotential height at that point by 10 m would change the response function by 0.06 Pa; therefore, a geopotential height perturbation of about 130 m is required to yield an equivalent change in the response function as a unit temperature perturbation at the same location.

A vertical cross-section through the adjoint sensitivity with respect to geopotential height shows an upshear-tilted pattern that is concentrated mainly in the lower troposphere (Fig. 7a). The sensitivity structure extends from just above the surface to near 500 hPa. The level of maximum sensitivity exists at sigma level 0.88, which is approximately 890 hPa.

These results, which show an upshear-tilted, lower-tropospheric structure in adjoint

sensitivity with respect to temperature and geopotential height are in broad agreement with previous studies on adjoint sensitivity and singular vectors applied to cyclogenesis (Errico and Vukicevic 1992, Langland et al. 1995, Rabier et al. 1996, Zou et al. 1998, Hoskins et al. 2000). The adjoint sensitivities here exhibit smaller horizontal scale than these previous studies, which may be due to the relatively smaller 45-km grid spacing used here, compared with approximately 100-km and greater used in most earlier studies.

4.b. Structure of Ensemble Sensitivities

Ensemble sensitivity is very different than the adjoint sensitivity in terms of scale, location, structure, and magnitude (Fig. 4). The ensemble sensitivities are synoptic scale and located near prominent weather features at the initial time. For example, a dipole of synoptic-scale ensemble sensitivity near 850 hPa is located under the area of maximum absolute vorticity at 500 hPa near 45° N, 150° W with positive values directly under the 500-hPa geopotential height trough, and negative values just downstream of the trough. There is also an elongated dipole of ensemble sensitivity near the surface just off the Pacific Northwest coast, which appears to be aligned along the low-level baroclinic zone at the initial time. At 500 hPa and above, large areas of positive ensemble sensitivity exist over the western North American continent. Furthermore, the ensemble sensitivities are not located solely in the interior of the lower half of the troposphere as are the adjoint sensitivities, but rather extend throughout the depth of the troposphere. Maximum ensemble sensitivity values of about 250 Pa/K imply that a unit temperature perturbation at that point, spread by the statistics of the initial-time analysis error covariance matrix changes the response function by 250 Pa.

Fig. 6 shows the ensemble sensitivity with respect to geopotential height at the same levels as in Fig. 4. The geopotential height field is much smoother than the corresponding field for the adjoint sensitivity field, and is dominated by a synoptic-scale dipole off the coast of the Pacific Northwest. This pattern has a maximum at the surface and decays upward as it tilts westward with height. At sigma level 12 (500 hPa), the synoptic-scale

region of positive sensitivity exists just downstream of the trough axis at the initial time. A vertical cross section through the area of greatest ensemble sensitivity also illustrates the deep structure, and gradual tilt with height (Fig. 7). The upshear tilt throughout the troposphere spans only about 500 km in the horizontal, compared to about 2000 km for the adjoint sensitivity field. Maximum sensitivity near the surface of about 15 Pa/m implies that a 10 m geopotential height perturbation, spread by the initial-time analysis error covariance matrix, changes the response function by about 150 hPa.

4.c. Accuracy of Adjoint and Ensemble Sensitivities

Here we test the accuracy of the sensitivity results by comparing the nonlinear evolution of perturbed initial conditions with the projection of the perturbation onto the adjoint sensitivity field and with the ensemble sensitivity. Perturbation initial conditions are defined by introducing a unit temperature change at a randomly selected grid point, and perturbing all other variables by the initial-time analysis-error covariance with this point. These perturbed fields are then added to the ensemble-mean initial condition, and run forward with the nonlinear model. This procedure is repeated for 20 different grid points, yielding the results shown in Fig. 8.

Differences in the response function between nonlinear solutions for the mean and perturbed fields provide nonlinear estimates of δJ. The predicted change in the forecast metric based on the ensemble sensitivity is given by the value of that field at the single point from which the perturbation was spread. The predicted change from the adjoint sensitivity field is given by the projection of the entire perturbation onto the adjoint sensitivity field. Differences among these δJ values are due to errors in the tangent-linear approximation, although sampling error may also exist for other forecast metrics. Results show good agreement between the ensemble and adjoint predictions, and the nonlinear result for δJ (Fig. 8). Although the ensemble results show slightly more scatter about the line of perfect agreement ($R^2 = 0.9775$) compared to the adjoint predictions ($R^2 = 0.9930$), it is clear that both provide accurate estimates of the changes in the forecast metric for the perturbation

considered here.

As mentioned previously, ensemble sensitivity analysis allows for straightforward application of statistical confidence measures to address sampling error. For example, Student T-tests may be performed on the ensemble sensitivity values to test whether the value is different than zero at a chosen confidence level (e.g. Wilkes 1995). Fig. 9 illustrates such a test by only displaying the ensemble sensitivity results for values that are different from zero at the 90% confidence level. Comparison with Fig. 4c indicates that most of the substantial ensemble sensitivity structure is significant with 90% confidence.

5. Discussion

5.a Interpretation of Adjoint and Ensemble Sensitivities

In order to understand the differences between the adjoint and ensemble sensitivity fields, we return to (14), which defines the fundamental relationship between them. The two approaches are equal only when the initial degrees of freedom are uncorrelated, in which case individual points may be considered independently. In reality, there are always non-zero correlations, which means that any change to one location must also be spread to other locations. Equivalently, the ensemble sensitivity is the projection of the analysis error covariance matrix onto the adjoint sensitivity field divided by the variance.

Here we explore the relationship between adjoint and ensemble sensitivity by way of illustration for the point of maximum ensemble sensitivity with respect to sigma level 22 (850 hPa) temperature, indicated by the black dot in Fig. 10a. Recall that the ensemble sensitivity at this point of about 250 Pa/K compares with the maximum value of adjoint sensitivity at this level of 0.8 Pa/K (Figs. 3c, 4c). Linear regression of the temperature field onto temperature at the point of maximum ensemble sensitivity (Fig. 10b) reveals significant relationships near the point, and also along the baroclinic zone further to the east and southeast; other longer-range relationships are likely suspect due to sampling error (cf. Fig. 9). These linear relationships correspond to a single row of the product of the

first two terms on the right-hand side of equation (14). Fig. 10d shows the product of the temperature perturbation (Fig. 10b) with the adjoint sensitivity field shown in Fig. 10c, which reveals the contribution of each point to the change in the forecast metric as estimated by the ensemble sensitivity value. This sum of projection values corresponds to a single row of the product of the first two terms on the right-hand side of equation (14) multiplied by the adjoint sensitivity vector. Since the adjoint sensitivity is small everywhere but a highly localized region located away from the point of maximum ensemble sensitivity, the product mainly reflects a weighted adjoint sensitivity field.

Within the easternmost box in Fig. 10d, which encompasses the small significant regions of adjoint sensitivity, the sum of the positive (negative) values is 12.45 Pa (−8.34 Pa), whereas for the westernmost box, which encompasses the large synoptic-scale region of positive ensemble sensitivity, the sum of the positive (negative) projections is 2.22 Pa (−1.09 Pa). Across the entire domain at this level, the positive (negative) contribution of the projection field is 20.63 Pa (−15.50 Pa), giving a net sum of 5.13 Pa; 4.11 Pa, or about 80%, comes from the region of significant adjoint sensitivities that occupies about 2% of the domain at this level. Thus when viewed from an adjoint sensitivity perspective, only the relatively small subspace of the ensemble sensitivity field that projects onto regions of significant adjoint sensitivity is important for changing the forecast metric.

5.b Application of Ensemble and Adjoint Sensitivities to Targeted Observations and Data Thinning

Assume for the moment that a single observation y is to be assimilated, that it is located at a model grid point with ensemble mean value x, and that it has zero error variance. In that case (28) reduces to

$$\delta J = \frac{\partial J_e}{\partial x}\,(y - x), \tag{32}$$

which shows that the change in the forecast metric is directly proportional to the ensemble sensitivity. Reintroducing the observation error variance simply scales the sensitivity value by a term involving both the background and observation variance, or more specifically,

results in the product of the ensemble sensitivity and the background variance at the point, normalized by the innovation variance. This result shows that the full ensemble sensitivity value as defined by (14) need not be calculated, and only the covariances between the metric and the model's estimate of the observation are necessary for assessing observation impact and data thinning. Although ensemble sensitivity could have been defined simply as these covariances, we note that an advantage of the adopted definition for the purposes of comparison in this paper is that ensemble sensitivity has the same units as adjoint sensitivity.

For targeting, only the observation error variance is known. For zero observation error variance, (22) reduces to

$$\delta\sigma \;=\; d\left(\frac{\partial J_e}{\partial x}\right)^2 . \tag{33}$$

Here, d is the background error variance at the location of the observation. Reintroducing the observation error variance again scales the square term in (22) by the square of the background variance normalized by the innovation variance. This term reduces to the square of the covariance between the metric and the model's estimate of the observation normalized by the innovation variance, again showing the necessity of only calculating covariances and not the full ensemble sensitivity value.

We now apply these ideas to the hypothetical targeting problem of identifying the location for a single temperature observation at sigma level 22, for an assumed observation error variance of 0.5 K^2. According to (22), the largest value in this field identifies the leading targeting location, which predicts a reduction in the response function variance of 1.3 hPa^2 (the control variance is 4.8 hPa^2) (Fig. 11a). The values of variance reduction plotted in Fig. 11 are only those which satisfy the 90% confidence interval as in Fig. 9, and observations should only be taken in locations which appear on the plots in Fig. 11 if this confidence level is to be satisfied. The primary targeting site is located at neither the region of maximum ensemble or adjoint sensitivity, but is somewhat closer to the local maximum in adjoint sensitivity.

Assuming the assimilation of an observation for the leading targeting location, the

second targeting priority can then be identified. The second targeting site is located just to the south of the maximum in ensemble sensitivity, and the predicted reduction in response function variance is about 0.3 hPa^2 (Fig. 11b). Further targeting locations may be determined conditioned on the first two, although with diminishing returns with respect to impact on the forecast response function variance.

6. Summary and Conclusions

Ensemble sensitivity is defined here by the linear regression of a forecast response function onto the initial conditions. We show that this field is proportional to the projection of the analysis-error covariance matrix onto the adjoint sensitivity field, and that the two are identical only when the initial degrees of freedom are uncorrelated. Expressions are derived using ensemble sensitivity to determine the impact of potential new observations on the response function variance (targeting) and on the response function expected value (observation impact and thinning).

Adjoint and ensemble sensitivity are compared for a response function defined by the 24-hour forecast of surface pressure at a single point in the Pacific Northwest region of the United Sates. Adjoint sensitivity patterns are small-scale, localized, lower-tropospheric structures that tilt strongly upshear, and are found away from major synoptic systems at the initial time. In contrast, ensemble sensitivity patterns are mostly synoptic scale, troposphere-deep structures that tilt modestly upshear, and are found close to major synoptic systems at the initial time. The largest ensemble sensitivity values are about two orders of magnitude greater than the largest adjoint sensitivity values, which is a consequence of the correlation between initial-time state variables. For a single point, adjoint sensitivity values must be summed over all points that covary with the point, in which case we find that the adjoint and ensemble predicted response function changes agree closely with each other, and with differences of nonlinear solutions for perturbed initial conditions. Consequently, for the point of greatest ensemble sensitivity we find that,

when viewed as a sum over covarying adjoint sensitivity locations, the main contribution to forecast metric changes come from locations of greatest adjoint sensitivity.

Expressions are derived for determining locations for targeted observations based on ensemble sensitivity fields. In the appropriate norm, this method is equivalent to the ensemble transform Kalman filter (ETKF), but does not require the determination of a transformation matrix, and also allows straightforward inclusion of statistical confidence measures to address sampling error. For the case considered, we find that the leading target site is located away from extrema in both the ensemble and adjoint sensitivity patterns, which is due to the fact that the response function variance is changed by a product of the ensemble sensitivity field with the analysis error variance. In other words, the targeting location is determined by the covariance between the response function and the initial degrees of freedom. A single observation of temperature with an assumed error variance of 0.5 K^2 predicts a reduction in the response function variance by about 25%. A second targeting site, conditional on having assimilated an observation from the first targeting site, predicts a further reduction in the response function variance of about 9%, with the location close to the maximum ensemble sensitivity.

These results suggest that the ensemble technique discussed here offers a straightforward and inexpensive approach to sensitivity analysis, observation targeting, and observation thinning. The performance of the ensemble technique for these problems over a larger sample of real cases will be explored elsewhere.

Acknowledgements: We thank Ryan Torn (University of Washington) for supplying the ensemble Kalman filter dataset on which our results are based, and for stimulating discussions on the topics in this paper. Discussions on the ETKF with Sharan Majumdar (University of Miami), which led to the results in Appendix A, are also gratefully acknowledged. This research was sponsored by the National Science Foundation through grant ITR-0205648 and by the National Oceanic and Atmospheric Administration through CSTAR grant NA17RJ1232.

Appendix A. Approximation of $\mathbf{A}^{-1}$ to recover adjoint sensitivity from ensemble sensitivity

An approximation of $\mathbf{A}^{-1}$ is needed to estimate adjoint sensitivity from multivariate ensemble regression (11). Since there are typically many fewer ensemble members than degrees of freedom, a pseudoinverse is determined by singular value decomposition, which is not unique (e.g. Press et al. 1993). A singular value decomposition of the analysis ensemble matrix $\mathbf{X}$ gives

$$\mathbf{X} = \mathbf{U}\mathbf{S}\mathbf{V}^{\mathrm{T}}, \tag{34}$$

where the dimensions of $\mathbf{U}, \mathbf{S}$, and $\mathbf{V}$ are NXN, NXM, and MXM, respectively. Substituting this expression for $\mathbf{X}$ into the expression for $\mathbf{A}$, noting that $\mathbf{U}$ and $\mathbf{V}$ are orthonormal matrices, and taking the inverse yields

$$\mathbf{A}^{-1} = \mathbf{U}\mathbf{S}^{-2}\mathbf{U}^{\mathrm{T}}. \tag{35}$$

Note that in computing the inverse of the diagonal matrix $\mathbf{S}$, only entries significantly different than zero are inverted.

A further simplification is available by replacing the calculation of the larger matrix $\mathbf{U}$ for the smaller matrix $\mathbf{V}$ as follows. The inner product $\mathbf{X}^{\mathrm{T}}\mathbf{X}$ leads to an eigenvector–eigenvalue problem for $\mathbf{S}$ and $\mathbf{V}$

$$\mathbf{X}^{\mathrm{T}}\mathbf{X}\mathbf{V} = \mathbf{V}\mathbf{S}^2, \tag{36}$$

and replacing $\mathbf{U}$ in favor of $\mathbf{V}, \mathbf{S}$ and $\mathbf{X}$ in (35) yields

$$\mathbf{A}^{-1} = \mathbf{X}\mathbf{V}\mathbf{S}^{-4}(\mathbf{X}\mathbf{V})^{\mathrm{T}}. \tag{37}$$

This result may then be used in (12), yielding an ensemble estimate of the adjoint sensitivity field.

References

Ancell, B. C., and C. F. Mass, 2006: Structure, growth rates, and tangent-linear accuracy of adjoint sensitivities with respect to horizontal and vertical resolution. *Mon. Wea. Rev.*, **134,** 2971-2988.

Baker, N., and R. Daley, 2000: Observation and background sensitivity in the adaptive observation-targeting problem. *Quart. J. Roy. Meteor. Soc.*, **126,** 1431–1454.

Barkmeijer, J., R. Buizza, and T. N. Palmer, 1999: 3D-VAR Hessian singular vectors and their potential use in the ECMWF ensemble prediction system. *Quart. J. Roy. Meteor. Soc.*, **125,** 2333–2351.

Berliner, M. L., Z-Q Lu, and C. Snyder, 1999: Statistical design for adaptive weather observations. *J. Atmos. Sci.*, **56,** 2536–2552.

Bishop, C. H., B. J. Etherton, and S. J. Majumdar, 2001: Adaptive sampling with the ensemble transform Kalman filter. Part I: Theoretical aspects. *Mon. Wea. Rev.*, **129,** 420–436.

Buizza, R., R. Gelaro, F. Molteni, and T. N. Palmer, 1997: The impact of increased resolution on predictability studies with singular vectors. *Quart. J. Roy. Meteor. Soc.*, **123,** 1007–1033.

Buizza, R., and A. Montani, 1999: Targeting observations using singular vectors. *J. Atmos. Sci.*, **56,** 2965–2985.

Ehrendorfer, M., and J. J. Tribbia, 1997: Optimal prediction of forecast error covariances through singular vectors. *J. Atmos. Sci.*, **54,** 286-313.

Errico, R. M., and T. Vukicevic, 1992: Sensitivity analysis using an adjoint of the PSU-NCAR mesoscale model. *Mon. Wea. Rev.*, **120,** 1644–1660.

Gelaro, R., R. H. Langland, G.D. Rohaly, and T.E. Rosmond, 1999: An assessment of the singular-vector approach to targeted observing using the FASTEX dataset. *Quart. J. Roy. Meteor. Soc.*, **125,** 3299–3327.

Hakim, G. J., 2005: Vertical structure of midlatitude analysis and forecast errors. *Mon. Wea. Rev.*, **132,** 567–578.

Hakim, G. J., and R. D. Torn, 2005: Ensemble synoptic analysis. Fred Sanders Monograph, American Meteorological Society.

Hamill, T. M., and C. Snyder, 2002: Using improved background-error covariances from an ensemble Kalman filter for adaptive observations. *Mon. Wea. Rev.*, **130,** 1552–1572.

Hamill, T. M., C. Snyder, and J. S. Whitaker, 2003: Ensemble forecasts and the properties of flow-dependent analysis-error covariance singular vectors. *Mon. Wea. Rev.*, **131,** 1741–1758.

Hartmann, D. L., R. Buizza, and T. N. Palmer, 1995: Singular vectors: The effect of spatial scale on linear growth of disturbances. *J. Atmos. Sci.*, **52,** 3885–3894.

Hoskins, B. J., R. Buizza, and J. Badger, 2000: The nature of singular vector growth and structure. *Quart. J. Roy. Meteor. Soc.*, **126,** 1565–1580.

Langland, R. H., R. L. Elsberry, and R. M. Errico, 1995: Evaluation of physical processes in an idealized extratropical cyclone using adjoint sensitivity. *Quart. J. Roy. Meteor. Soc.*, **121,** 1349–1386.

Langland, R. H., Z. Toth, R. Gelaro, I. Szunyhogh, M. A. Shapiro, S. J. Majumdar, R. E. Morss, G. D. Rohaly, C. Velden, N. Bond, and C. H. Bishop, 1999: The North Pacific Experiment (NORPEX-98): Targeted observations for improved North American weather forecasts. *Bull. Amer. Meteor. Soc.*, **180,** No. 7, 1363–1384.

Langland, R. H., and N. L. Baker, 2004: Estimation of observation impact using the NRL atmospheric variational data assimilation adjoint system. *Tellus*, **56A,** 189–201.

LeDimet, F, and O. Talagrand, 1986: Variational algorithms for analysis and assimilation of meteorological observations: Theoretical aspects. *Tellus*, **38A,** 97–110.

Majumdar, S. J., C. H. Bishop, B. J. Etherton, I. Szunyogh, and Z. Toth, 2001: Can an ensemble transform Kalman filter predict the reduction in forecast-error variance produced by targeted observations? *Quart. J. Roy. Meteor. Soc.*, **127,** 2803–2820.

Majumdar, S. J., C. H. Bishop, and B. J. Etherton, 2002: Adaptive sampling with the ensemble transform Kalman filter. Part II: Field program implementation. *Mon. Wea. Rev.*, **130,** 1356–1369.

Palmer, T.N., R. Gelaro, J. Barkmeijer, and R. Buizza, 1998: Singular vectors, metrics, and adaptive observations. *J. Atmos. Sci.*, **55,** 633–653.

Press, W. H. , B. P. Flannery, and S. A. Teukolsky, 1993: Numerical recipes in FORTRAN: The art of scientific computing. Cambridge University Press, 992 pp.

Rabier, F., E. Klinker, P. Courtier, and A. Hollingsworth, 1996: Sensitivity of forecast errors to initial conditions. *Quart. J. Roy. Meteor. Soc.*, **122,** 121–150.

Ruggiero, Frank H., G.D. Modica, T. Nehrkorn, M. Cerniglia, J.G. Michalakes, and X. Zou, 2002: Beta test code documentation for CWO-5. Air Force Research Laboratory, 1–23.

Snyder, C., and G. J. Hakim, 2005: Cyclogenetic perturbations and analysis errors decomposed into singular vectors. *J. Atmos. Sci.*, **61,** in press.

Torn, R. D., G. J. Hakim, and C. Snyder, 2006: Boundary conditions for limited-area ensemble Kalman filters. *Mon. Wea. Rev.*, **134,** 2490–2502.

Wilkes, D. S., 1995: *Statistical Methods in the Atmospheric Sciences.* Academic Press, 464.

Zou, X., Y.-H. Kuo, and S. Low-Nam, 1998: Medium-range prediction of an extratropical oceanic cyclone: impact of initial state. *Mon. Wea. Rev.*, **126,** 2737–2763.

Figure Captions

Figure 1. 500-hPa absolute vorticity (dashed lines, contour interval is 4×10^{-5} s^{-1}, countours begin at 12×10^{-5} s^{-1}) and 500-hPa geopotential height (solid lines, contour interval is 60 m) forecast at a) 00 hr, b) 12 hr, and c) 24 hr initialized from the ensemble mean initial condition at 1200 UTC 3 February 2005.

Figure 2. Sea-level pressure (solid lines, contour interval is 4 hPa) and 925-hPa temperature (dashed lines, contour interval is 4° C) forecast at a) 00 hr, b) 12 hr, and c) 24 hr initialized from the ensemble mean initial condition at 1200 UTC 3 February 2005.

Figure 3. Adjoint sensitivity of the response function with respect to initial temperature (thick lines) and basic-state temperature field (thin lines) at 1200 UTC 3 February 2005 at sigma levels a) 7 (300 hPa), contour interval 0.05 Pa/K, b) 12 (500 hPa), contour interval 0.05 Pa/K, and c) 22 (850 hPa), contour interval is 0.1 Pa/K. Solid lines denote positive values, dashed lines denote negative values.

Figure 4. Ensemble sensitivity of the response function with respect to initial temperature (thick lines) and basic-state temperature field (thin lines) at 1200 UTC 3 February 2005 at sigma levels a) 7 (300 hPa), b) 12 (500 hPa), c) 22 (850 hPa), and d) 32 (surface). Solid lines denote positive values, dashed lines denote negative values, contour interval is 50 Pa/K.

Figure 5. Adjoint sensitivity of the response function with respect to initial geopotential height (thick lines) and basic-state geopotential height field (thin lines) at 1200 UTC 3 February 2005 at sigma levels a) 7 (300 hPa), contour interval is 0.0005 Pa/m, b) 12 (500 hPa), contour interval is 0.0005 Pa/m, and c) 22 (850 hPa), contour interval is 0.001 Pa/m. Solid lines denote positive values, dashed lines denote negative values.

Figure 6. Ensemble sensitivity of the response function with respect to initial geopotential height (thick lines) and basic-state geopotential height or sea-level pressure

field (thin lines) at 1200 UTC 3 February 2005 at sigma levels a) 7 (300 hPa), b) 12 (500 hPa), c) 22 (850 hPa), and d) 32 (surface). Solid lines denote positive values, dashed lines denote negative values, contour interval is 3 Pa/m.

Figure 7. Cross-section of a) adjoint sensitivity (cross-section location shown in Fig. 5), contour interval is 0.001 Pa/m, and b) ensemble sensitivity (cross-section location shown in Fig. 6), contour interval is 3 Pa/m, of the response function with respect to initial geopotential height at 1200 UTC 3 February 2005. Solid lines denote positive values, dashed lines denote negative values.

Figure 8. Plot of the change in response function associated with both the statistical projection onto the adjoint sensitivity field (denoted by the symbol o) and the ensemble sensitivity (denoted by the symbol x) versus the nonlinear change in response function for a statistically-spread unit temperature perturbation made at twenty grid points throughout the model domain.

Figure 9. Ensemble sensitivity of the response function with respect to initial temperature at 1200 UTC 3 February 2005 at sigma level 22 (850 hPa) calculated at the 90% confidence interval. Solid lines denote positive values, dashed lines denote negative values, contour interval is 50 Pa/K.

Figure 10. a) Ensemble sensitivity of the response function with respect to initial temperature, contour interval is 50 Pa/K, b) a unit temperature perturbation made at the black dot in the ensemble sensitivity field and spread by the initial error covariance statistics, contour interval is 0.5 K, c) the adjoint sensitivity of the response function with respect to initial temperature, contour interval is 0.1 Pa/K, and d) the projection of the statistically-spread perturbation onto the adjoint sensitivity, contour interval is 0.1 Pa at sigma 22 (850 hPa) at 1200 UTC 3 February 2005. Solid lines denote positive values, dashed lines denote negative values.

Figure 11. Reduction in response function variance from the assimilation of a) a single observation at sigma level 22 (850 hPa), contour interval is 2000 Pa^2, and b) a second single observation at sigma level 22 (850 hPa), contour interval is 800 Pa^2, given the simultaneous assimilation of the observation near 42° N, 138° W in panel (a) associated with the largest response function variance reduction at 1200 UTC 3 February 2005. Only the variance reduction values that are calculated with the ensemble sensitivities which satisfy the 90% confidence interval in Fig. 9 are shown.

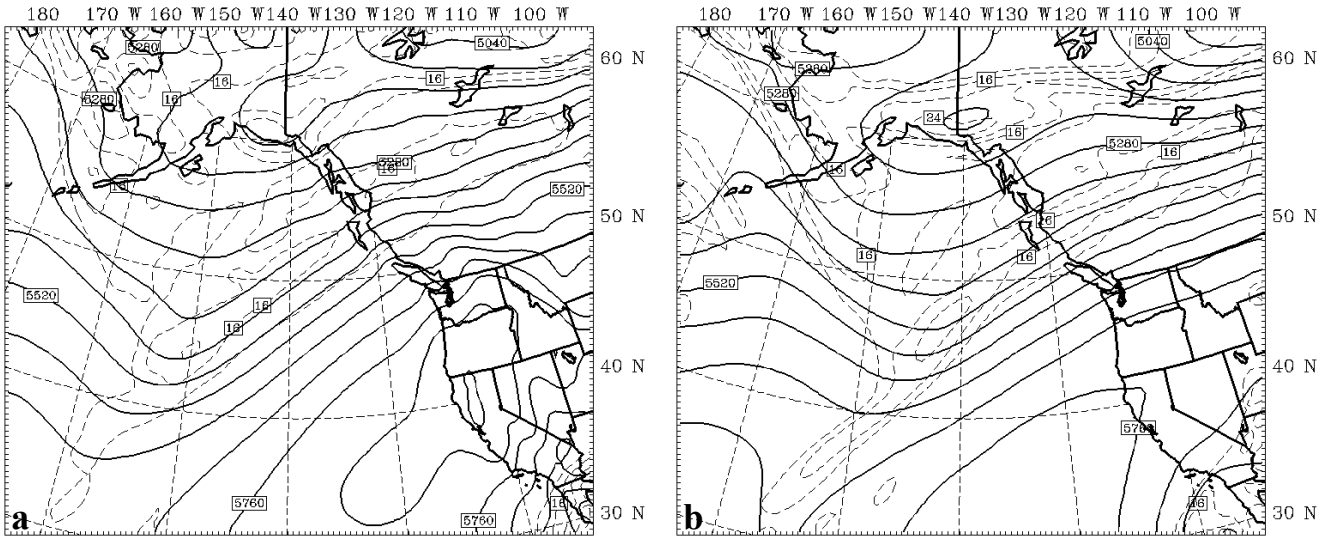

1200 UTC February 3 0000 UTC February 4

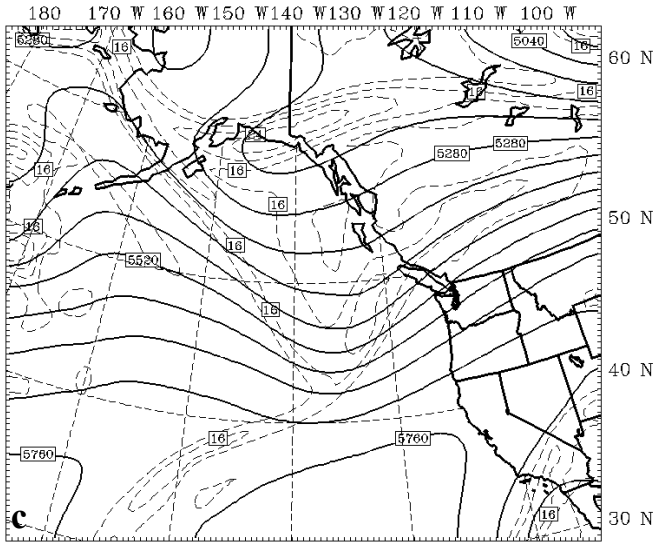

1200 UTC February 4

Figure 1. 500-hPa absolute vorticity (dashed lines, countour interval is $4x10^{-5}$ s^{-1}, contours begin at $12x10^{-5}$ s^{-1}) and 500-hPa geopotential height (solid lines, contour interval is 60 m) forecast at a) 00 hr, b) 12 hr, and c) 24 hr initialized from the ensemble mean initial condition at 1200 UTC 3 February 2005.

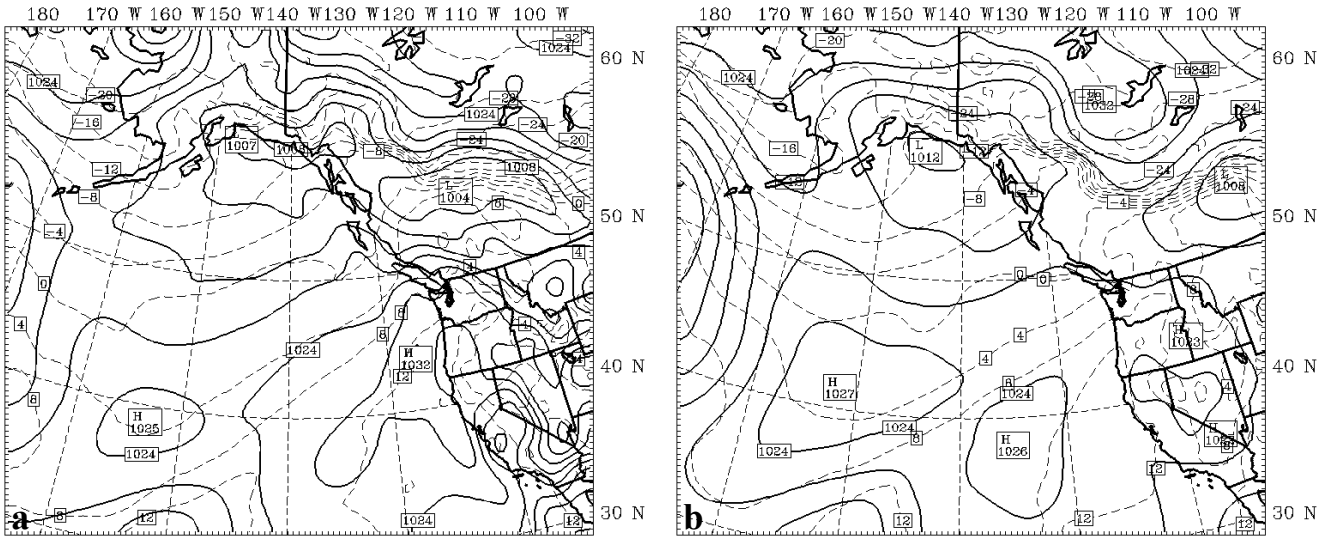

1200 UTC February 3 0000 UTC February 4

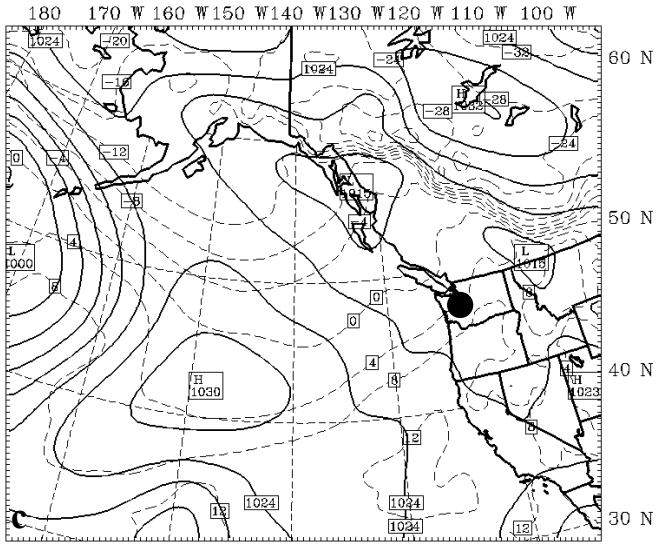

1200 UTC February 4

Figure 2. Sea-level pressure (solid lines, contour interval is 4 hPa) and 925-hPa temperature (dashed lines, contour interval is 4 ^{o}C) forecast at a) 00 hr, b) 12 hr, and c) 24 hr initialized from the ensemble mean initial condition at 1200 UTC 3 February 2005.

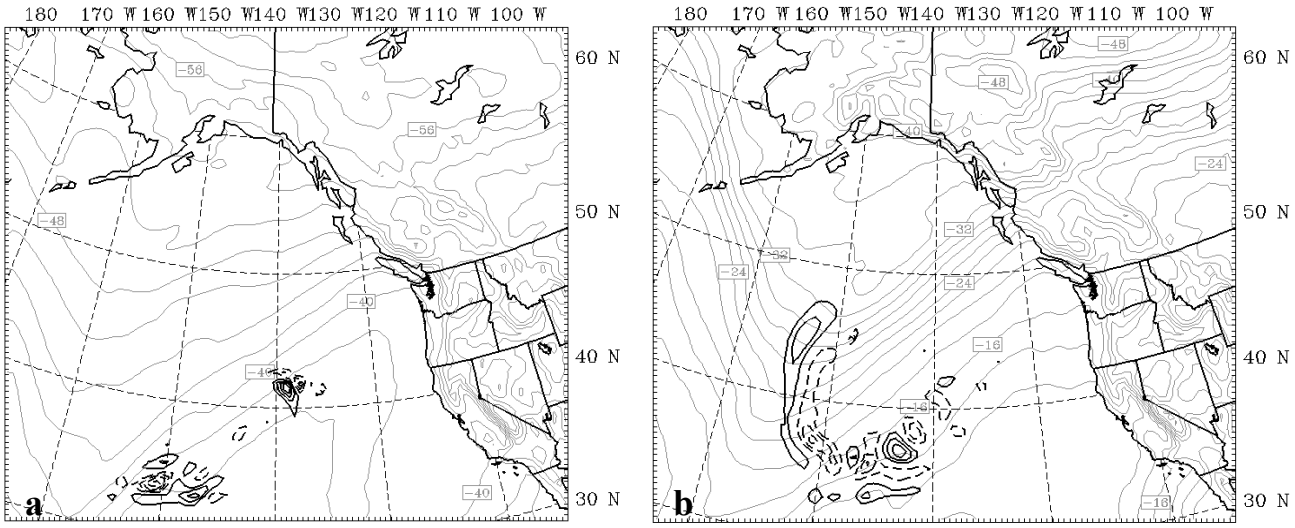

Sigma 7 (300 hPa) Sigma 12 (500 hPa)

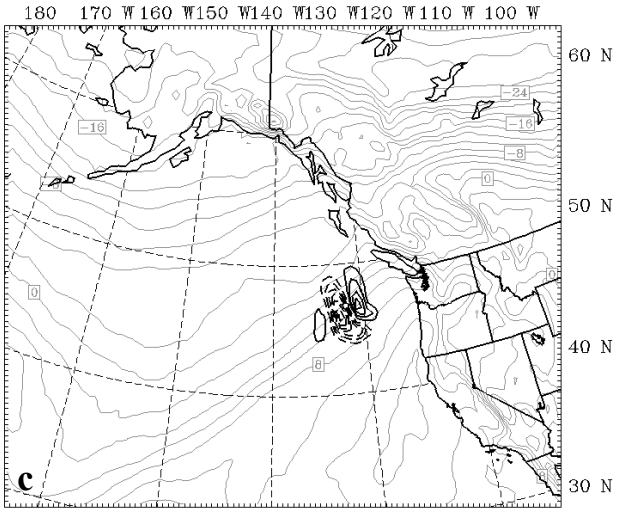

Sigma 22 (850 hPa)

Figure 3. Adjoint sensitivity of the response function with respect to initial temperature (thick lines) and basic-state temperature field (thin lines) at 1200 UTC 3 February 2005 at sigma levels a) 7 (300 hPa), contour interval is 0.05 Pa/K, b) 12 (500 hPa), contour interval is 0.05 Pa/K, and c) 22 (850 hPa), contour interval is 0.1 Pa/K. Solid lines denote positive values, dashed lines denote negative values.

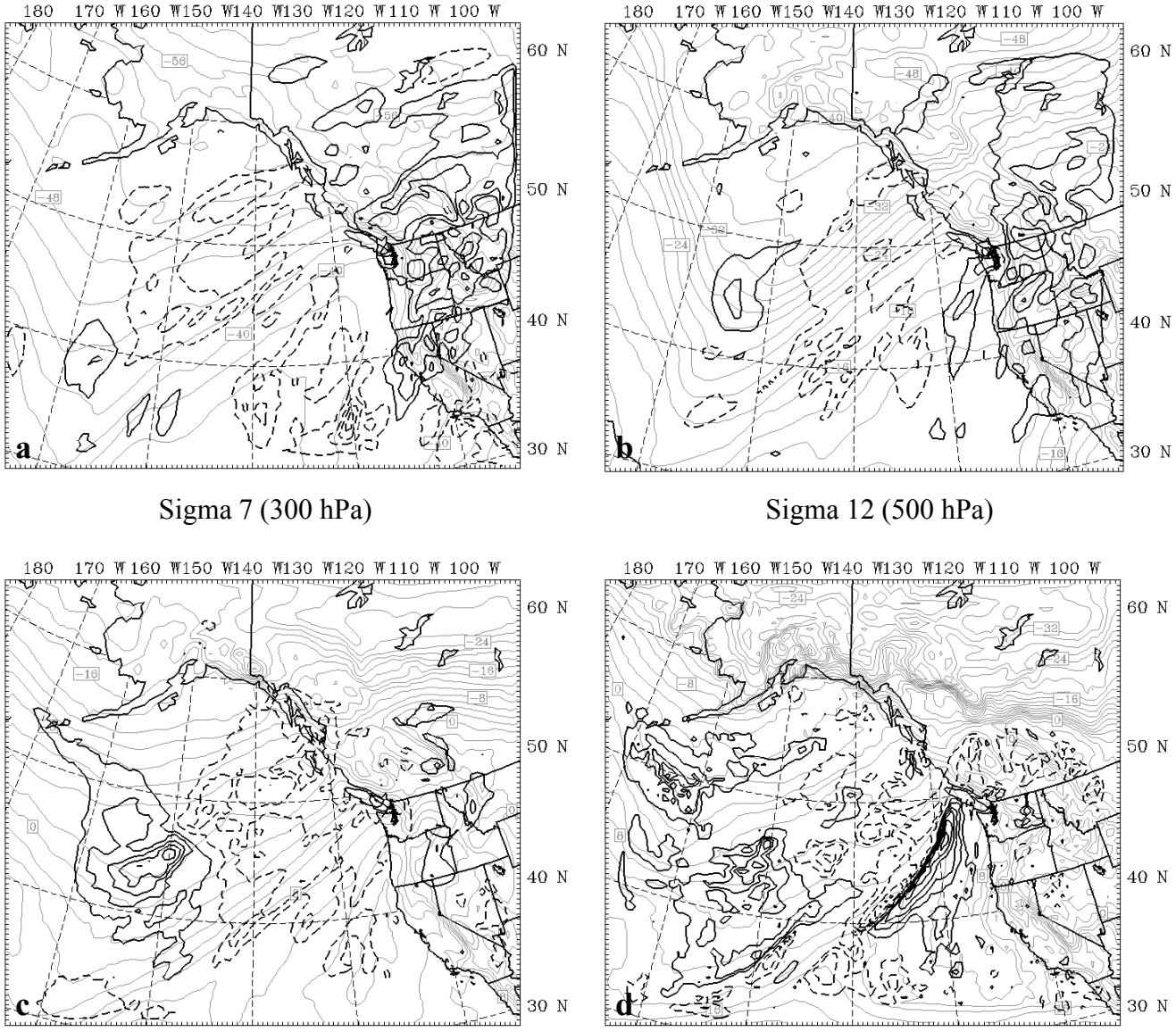

Sigma 7 (300 hPa)

Sigma 12 (500 hPa)

Sigma 22 (850 hPa)

Sigma 32 (surface)

Figure 4. Ensemble sensitivity of the response function with respect to initial temperature (thick lines) and basic-state temperature field (thin lines) at 1200 UTC 3 February 2005 at sigma levels a) 7 (300 hPa), b) 12 (500 hPa), c) 22 (850 hPa), and d) 32 (surface). Solid lines denote positive values, dashed lines denote negative values, contour interval is 50 Pa/K.

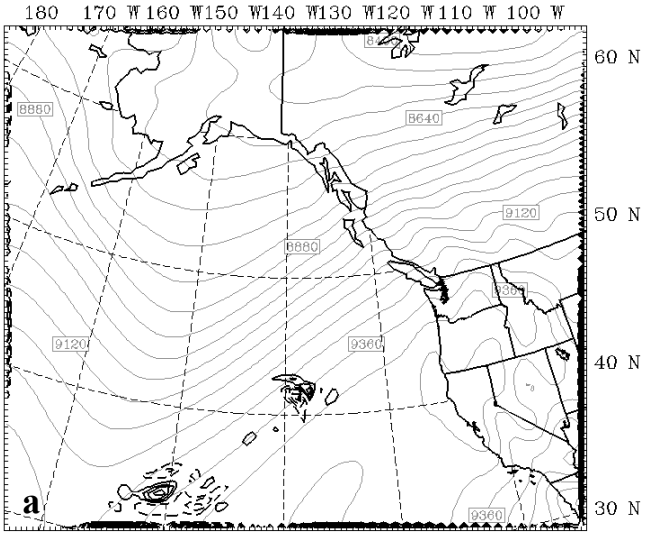

Sigma 7 (300 hPa)

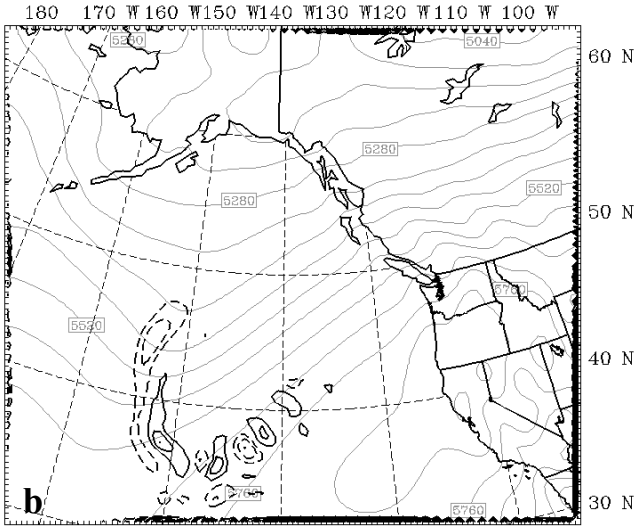

Sigma 12 (500 hPa)

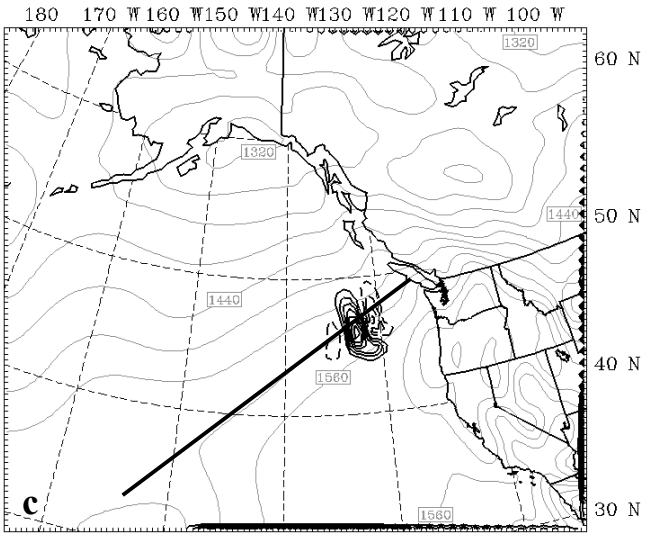

Sigma 22 (850 hPa)

Figure 5. Adjoint sensitivity of the response function with respect to initial geopotential height (thick lines) and basic-state geopotential height field (thin lines) at 1200 UTC 3 February 2005 at sigma levels a) 7 (300 hPa), contour interval is 0.0005 Pa/m, b) 12 (500 hPa), contour interval is 0.0005 Pa/m, and c) 22 (850 hPa), contour interval is 0.001 Pa/m. Solid lines denote positive values, dashed lines denote negative values.

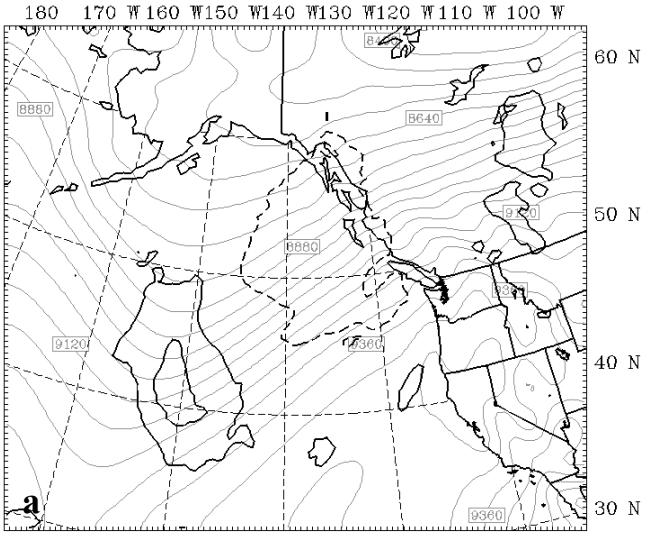

Sigma 7 (300 hPa)

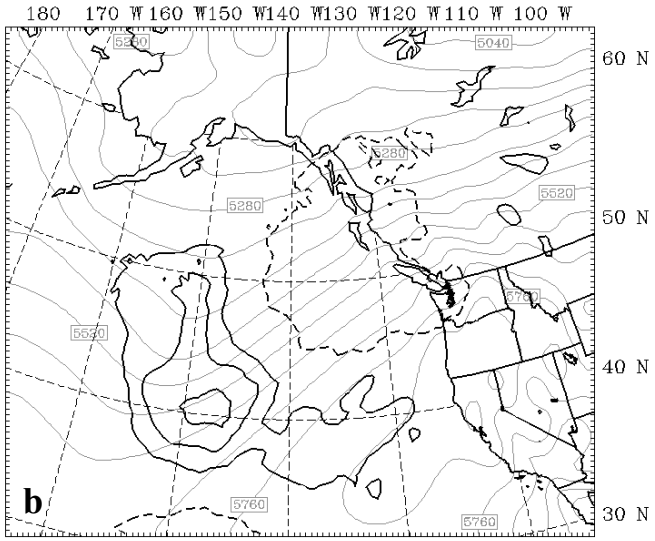

Sigma 12 (500 hPa)

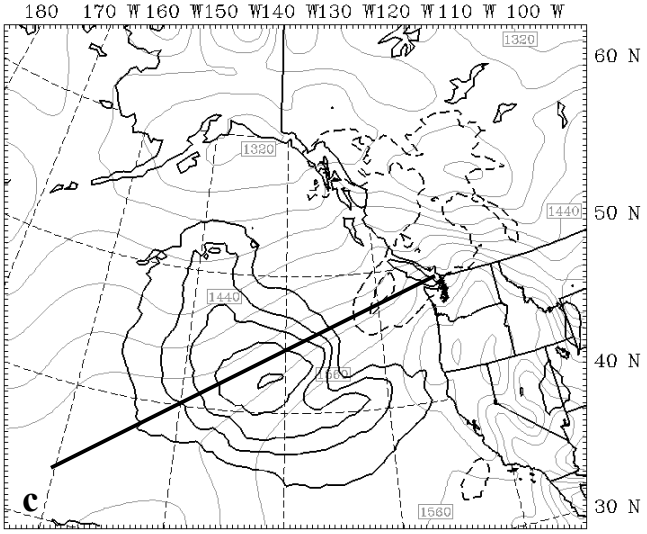

Sigma 22 (850 hPa)

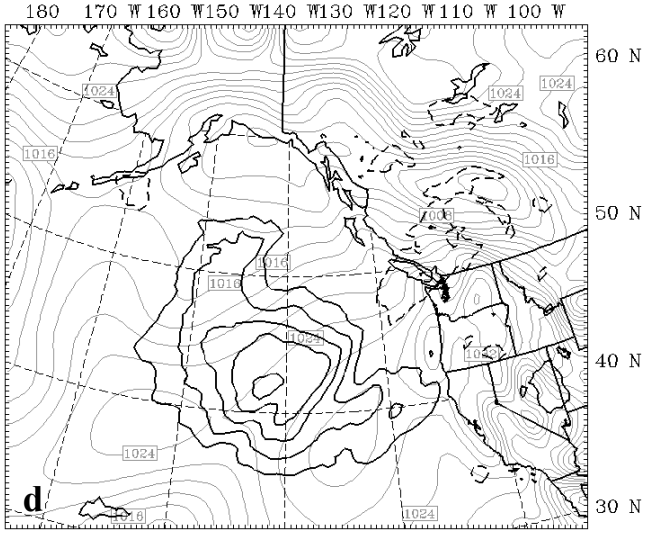

Sigma 32 (surface)

Figure 6. Ensemble sensitivity of the response function with respect to initial geopotential height (thick lines) and basic-state geopotential height or sea-level pressure field (thin lines) at 1200 UTC 3 February 2005 at sigma levels a) 7 (300 hPa), b) 12 (500 hPa), c) 22 (850 hPa), and d) 32 (surface). Solid lines denote positive values, dashed lines denote negative values, contour interval is 3 Pa/m.

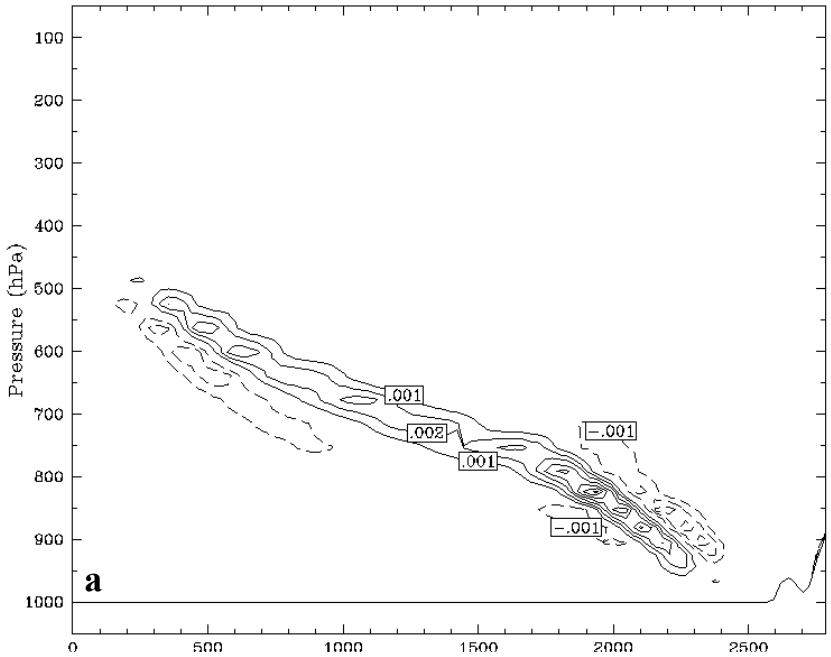

Adjoint sensitivity

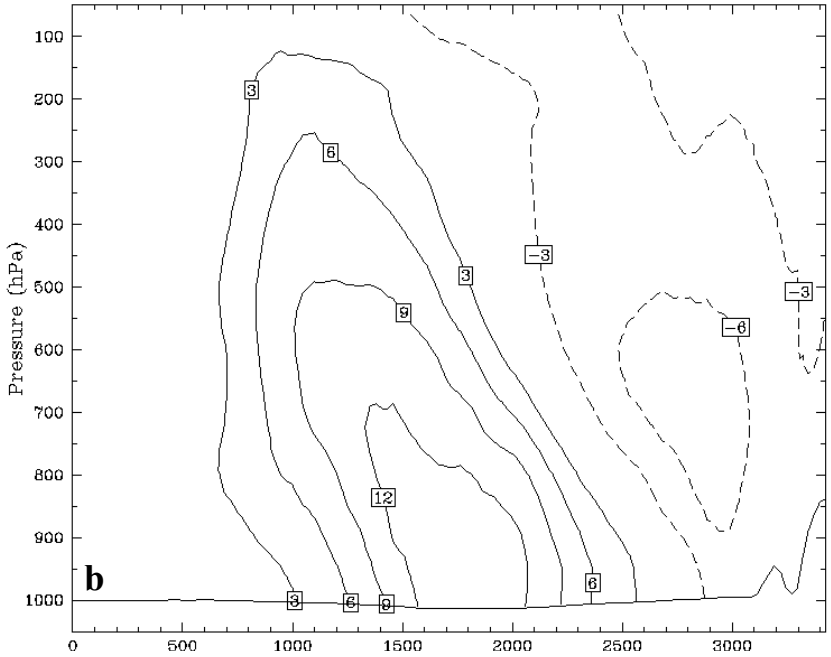

Ensemble sensitivity

Figure 7. Cross-section of a) adjoint sensitivity (cross-section location shown in Fig. 5), contour interval is 0.001 Pa/m, and b) ensemble sensitivity (cross-section location shown in Fig. 6), contour interval is 3 Pa/m, of the response function with respect to initial geopotential height at 1200 UTC 3 February 2005. Solid lines denote positive values, dashed lines denote negative values.

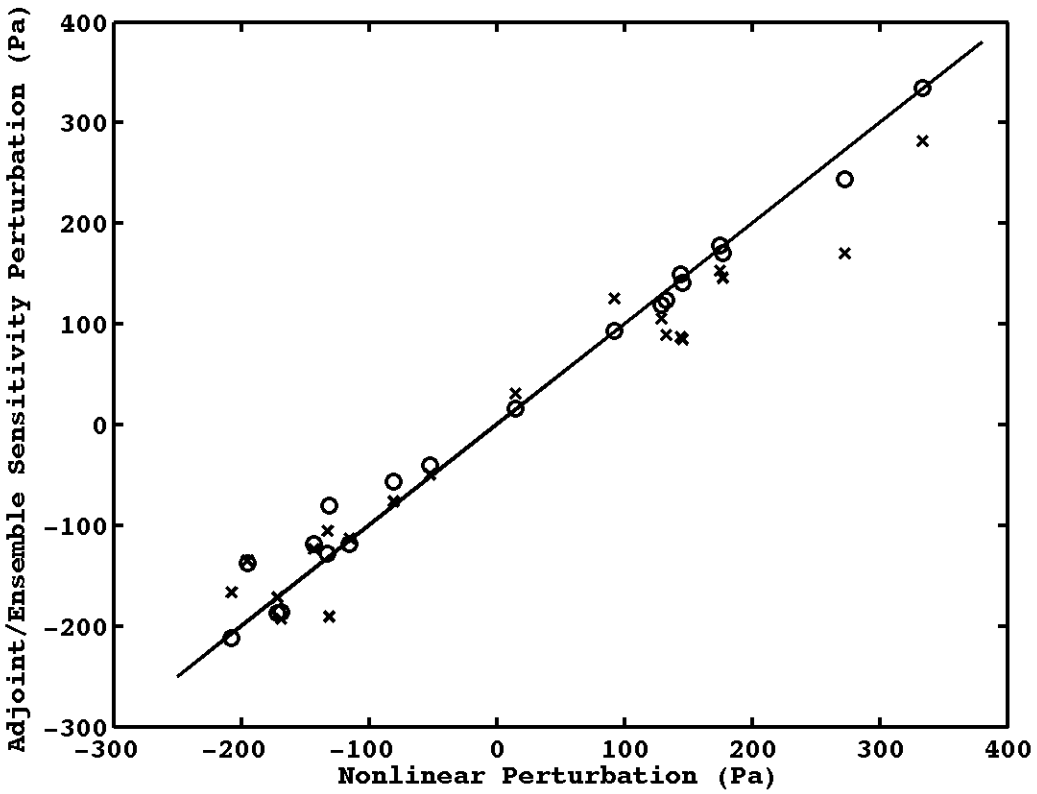

Figure 8. Plot of the change in response function associated with both the statitistical projection onto the adjoint sensitivity field (denoted by the symbol o) and the ensemble sensitivity (denoted by the symbol x) versus the nonlinear change in response fucntion for a statistically-spread unit temperature perturbation made at twenty grid points throughout the model domain.

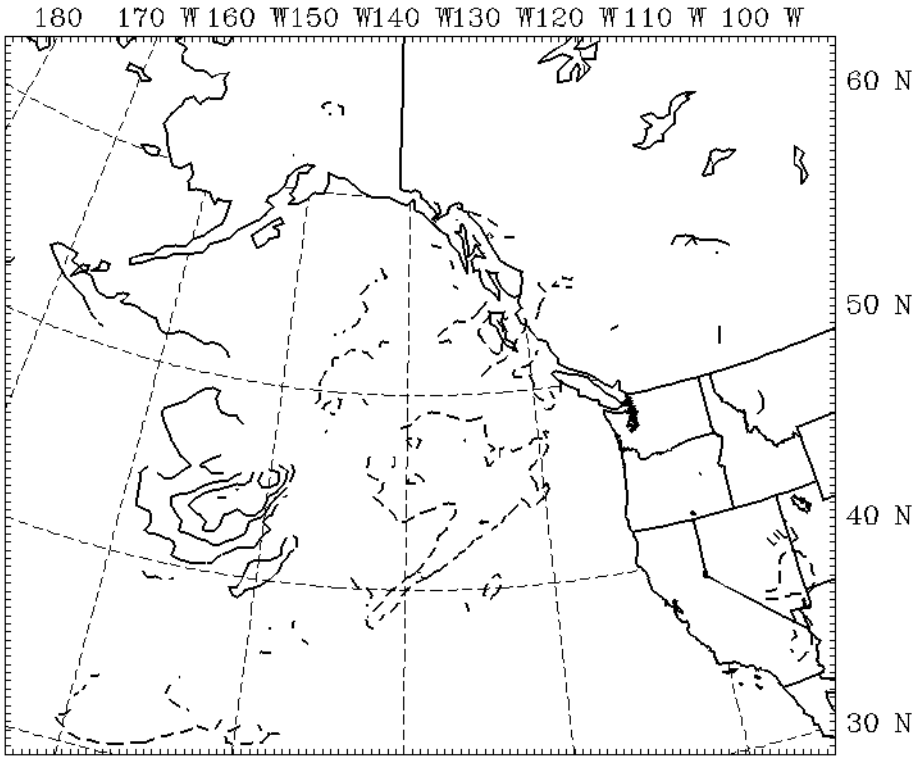

Figure 9. Ensemble sensitivity of the response function with respect to initial temperature at 1200 UTC 3 February 2005 at sigma level 22 (850 hPa) calculated at the 90% confidence interval. Solid lines denote positive values, dashed lines denote negative values, contour interval is 50 Pa/K.

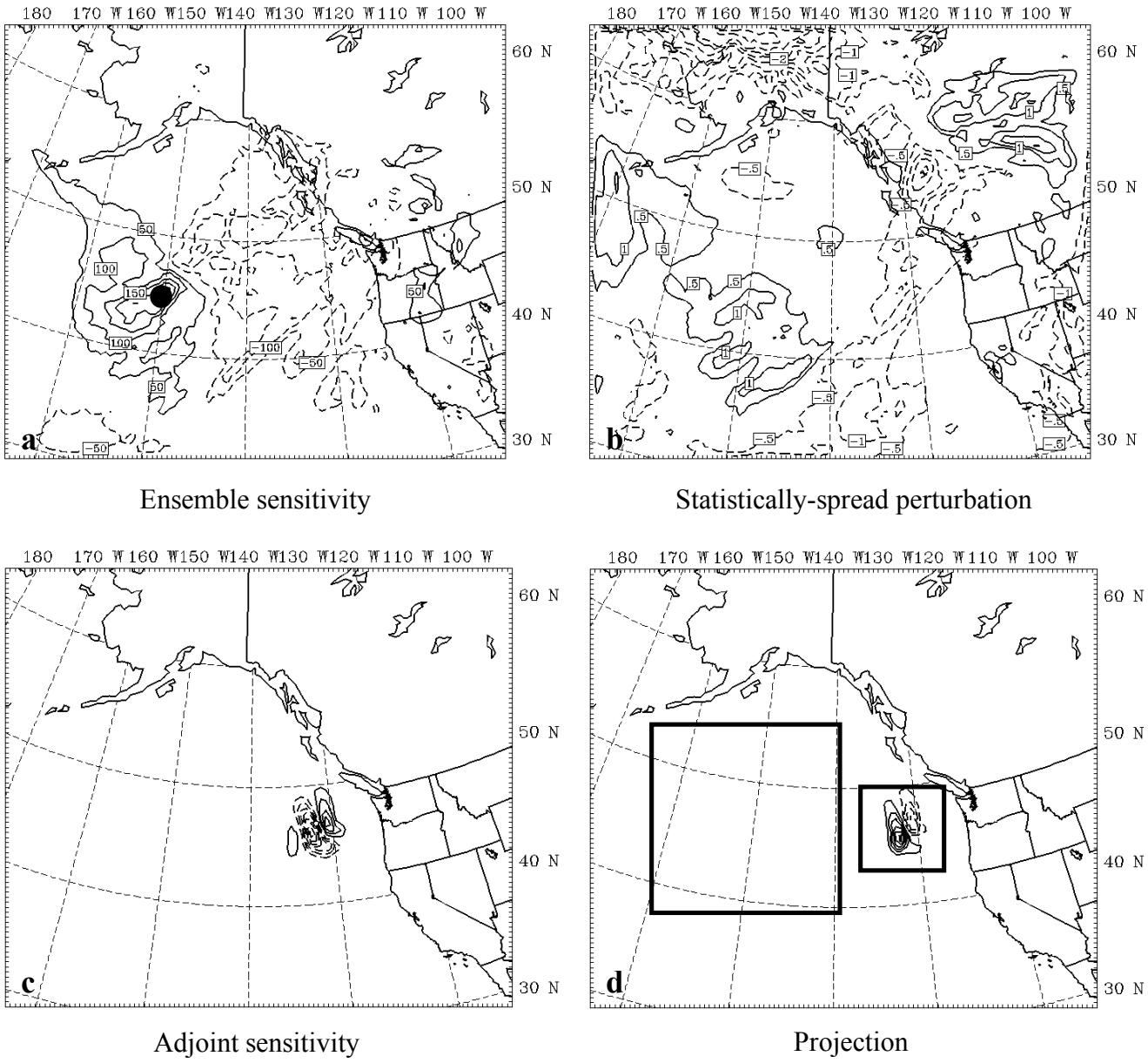

Figure 10. a) Ensemble sensitivity of the response function with respect to initial temperature, contour interval is 50 Pa/K, b) a unit temperature perturbation made at the black dot in the ensemble sensitivity field and spread by the initial error covariance statistics, contour interval is 0.5 K, c) the adjoint sensitivity of the response function with respect to initial temperature, contour interval is 0.1 Pa/K, and d) the projection of the statistically-spread perturbation onto the adjoint sensitivity, contour interval is 0.1 Pa at sigma 22 (850 hPa) at 1200 UTC 3 February 2005. Solid lines denote positive values, dashed lines denote negative values.

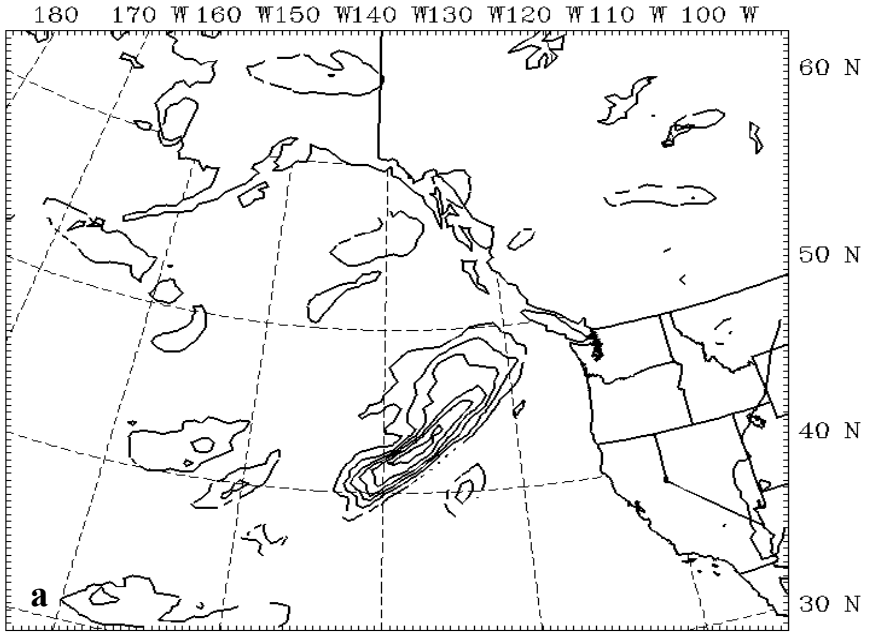

First observation

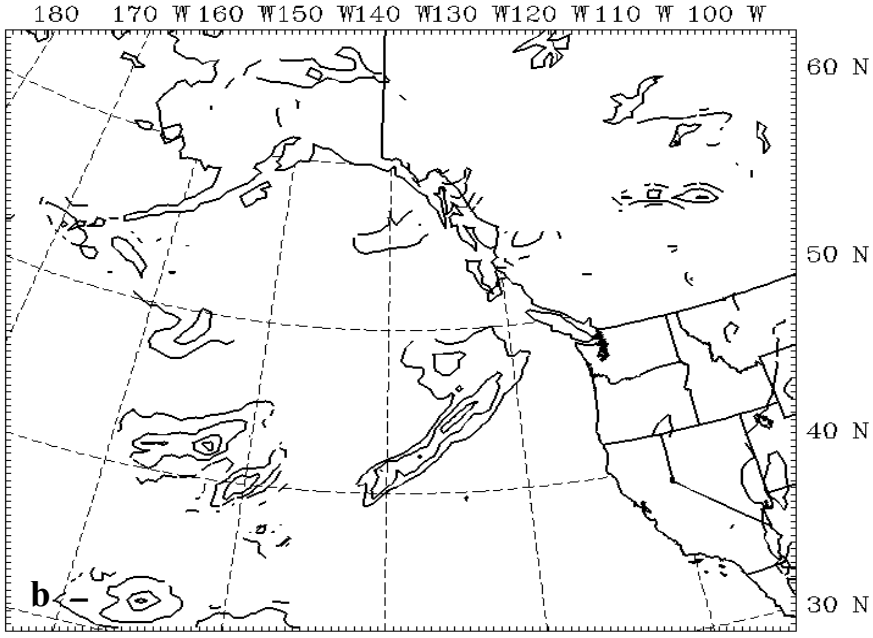

Second observation

Figure 11. Reduction in response function variance from the assimlation of a) a single observation at sigma level 22 (850 hPa), contour interval is 2000 Pa^2, and b) a second single observation at sigma level 22 (850 hPa), contour interval is 800 Pa^2,given the simultaneous assimilation of the observation near 42 N, 138 W in panel (a) associated with the largest response function variance reduction at 1200 UTC 3 February 2005. Only the variance reduction values that are calculated with the ensemble sensitivities which satisfy the 90% confidence interval in Fig. 9 are shown.